Proceedings of the 11th World Congress on Electrical Engineering and Computer Systems and Sciences (EECSS'25)
Paris, France - August, 2025
Paper No. EEE 107
DOI: 10.11159/eee25.107

Health Status Classification of Electric Motors Using CNN-Based Models and SDP Images Under Varying Noise Conditions

Merve Ertarğın[1], Nikolay Yordanov[2], Marin Zhilevski[2]
[1] University of Munzur
Department of Electrical and Electronics Engineering, Tunceli, Türkiye
merveboydak@munzur.edu.tr;
[2]Technical University of Sofia
Faculty of Automatics, Sofia, Bulgaria
nikolayyordanov@tu-sofia.bg;
[2] Technical University of Sofia
Faculty of Automatics, Sofia, Bulgaria
mzhilevski@tu-sofia.bg

Abstract **-** The increasing application of electric motors across various industrial sectors requires effective monitoring and early diagnostics to prevent potential failures. This study explores the use of Convolutional Neural Network (CNN)-based models together with Symmetrized Dot Pattern (SDP) sound representations for classifying the health status of electric motors under different noise conditions. Acoustic data from a brushless DC motor were transformed into SDP images, which were then used to train CNN models. The dataset included recordings of motors in "Good", "Broken" and "Heavy Load" conditions, captured under various noise environments such as pure, talking, white noise, atmospheric, and stress test conditions. The classification tasks were conducted under three conditions: assessing motor health status, evaluating both motor health status and noise types, and excluding the stress test noise type for a balanced dataset. The results demonstrated that the CNN models achieved high accuracy rates in classifying motor health status, with the Custom CNN model performing best in simpler tasks and MobileNet excelling in more complex scenarios. The study highlights the feasibility of using SDP images with CNN-based models for fault classification in motors and suggests future research directions for improving classification accuracy through advanced feature extraction techniques and multimodal data representations.

Keywords**:** electric motor, classification, acoustic data, SDP method, CNN-based models.

1. Introduction

In recent decades, there has been a global trend towards the increasing application of electric motors in various industrial sectors, thanks to their advantages in terms of efficiency and precision. They are characterized by a wide range of power, speed, and other key parameters. Electric drives find applications in all industrial sectors, including energy, mechanical engineering, metal and woodworking, food processing, pharmaceuticals, as well as in the textile, pulp, construction, and other sectors [1, 2].

On the other hand, electric motors are prone to various faults, including rotor asymmetries, bearing failures, and insulation degradation [3 - 5]. That's why the monitoring and the early diagnostics are of great importance for eliminating potential failures and malfunctions. This, in turn, leads to increased productivity, reliability, and operational safety of electric drive systems.

Traditional fault detection methods often rely on vibration analysis, current signature analysis, or thermal monitoring [6, 7]. Different types of fault detections and diagnosis with acoustic signals together image classification using neural networks are presented and analyzed in [8, 9]. The SDP method stands out due to its ability to visualize complex periodic and aperiodic signal behaviors in a compact graphical form, allowing for easier fault identification. The SDP technique has been successfully applied to detect various motor faults, including: rotor faults: cracked or broken rotor bars manifest as distortions in the pattern's symmetry; bearing faults: localized defects in bearings produce irregular dot clusters or noise-like features; stator faults: winding imbalances or insulation failures disrupt the uniformity of the dot distribution [10 - 15].

Machine learning and artificial intelligence represent modern methods for applying techniques and algorithms for monitoring and diagnosing electric drive systems, offering enhanced accuracy and efficiency compared to traditional approaches. These methods leverage advanced algorithms, such as neural networks, decision trees, and ensemble techniques, to process large datasets and extract meaningful patterns related to system health. In particular, CNNs have demonstrated high effectiveness in analyzing images obtained through signal processing techniques for fault detection and classification.

This study, focuses on how acoustic data can be represented and utilized for detecting faults in electric motors. The study explores various methods for collecting and processing acoustic signals, and how these can be analyzed using machine learning models to identify potential defects with corresponding probabilities of occurrence.

2. Dataset

The SDP technique transforms time-domain signals into two-dimensional dot patterns based on signal amplitude and phase relationships. The process involves: Signal Transformation: vibration or current signals are sampled and normalized; Dot Pattern Formation: consecutive points in the signal are plotted in a symmetrical arrangement to reveal periodic features and anomalies; Fault Analysis: patterns are evaluated for distortions, asymmetries, or irregularities indicative of faults [10].

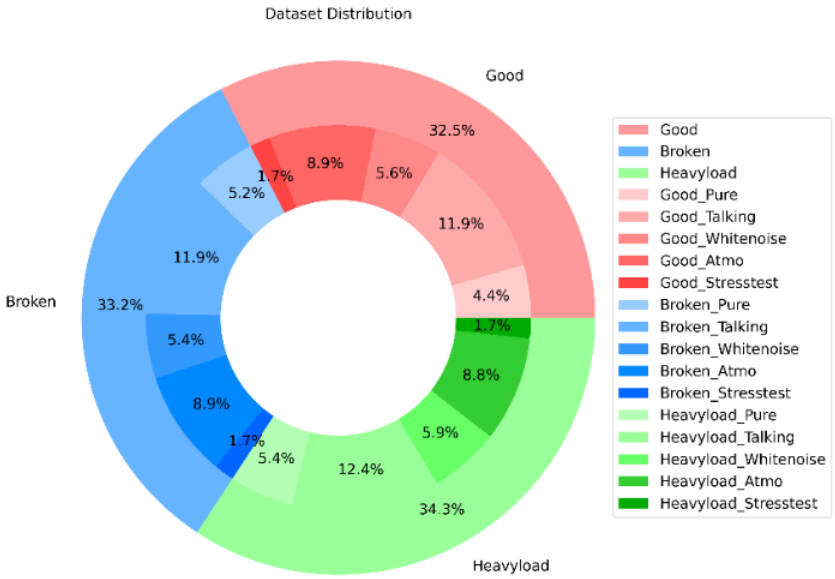

Fig. 1: Dataset distribution.

For this experiment, the IDMT-ISA-ELECTRIC-ENGINE Dataset was utilized [16]. The dataset was split into training, validation, and testing subsets. Sound recordings generated by the ACT DC Brushless Motor 42BLF01, operating at 4000 RPM and 24VDC, were included. The recordings were captured using an improvised microphone with the following specifications: frequency range of 50 Hz to 20 kHz, voltage range of 2 V to 10 V, omnidirectional, and sensitivity of −35 dB ± 4 dB.

Recordings of three different motor conditions were included in the dataset:

1. **Good Condition**: The first motor was operated at 60% of the supply voltage, representing the “good” working condition.
2. **Broken Condition**: The second motor's supply voltage was varied every 18ms between 15% and 75% to simulate a “broken” condition.
3. **Heavy Load Condition**: The third motor was subjected to an additional load, with a supply voltage of 60% of the nominal value, to represent the “heavy load” condition.

Recordings of electric DC motors operating in various sound environments were featured in the dataset, including:

- **Pure**: Recordings without the presence of other sounds or noise (no domain-shift).
- **Talking**: Recordings with the presence of audible conversations near the case surrounding the device.
- **White Noise**: Recordings with background white noise generated by nearby speakers.
- **Atmo**: Recordings with sounds from a factory environment emitted by speakers in three volume levels (low, medium, high).
- **Stress Test**: Recordings with controlled variations in loudness.

Figure 1 shows the dataset distribution across different motor health conditions and their associated noise types. The outer ring represents the health conditions, while the inner ring shows the detailed distribution of noise types within each health condition. The "good" health condition accounts for 32.5% of the data, followed by "broken" with 33.2% and "heavyload" with 34.3%.

Table 1 provides the dataset distribution after splitting into training (80%), validation (10%), and test (10%) sets based on motor health status and noise types. The training set contains a total of 1,896 samples, distributed as 617 for "good" 629 for "broken" and 650 for "heavyload". The validation set has 236 samples and test set has a total of 246 samples. Among noise types, "talking" has the highest number of samples across all splits, while "stresstest" has the lowest number, reflecting the dataset's inherent imbalance in noise distribution.

Table 1: Dataset after splitting.

Noise Type	**Train (%80)**			**Validation (%10)**			**Test (%10)**		
	Good	Broken	Heavyload	Good	Broken	Heavyload	Good	Broken	Heavyload
Pure	84	99	102	10	12	13	11	13	13
Talking	225	226	236	28	28	30	29	29	30
Whitenoise	107	103	112	13	13	14	14	13	14
Atmo	169	169	168	21	21	21	22	22	21
Stresstest	32	32	32	4	4	4	5	5	5
Total	617	629	650	76	78	82	81	82	83

3. Experimental Results

The classification task was conducted under three different conditions to evaluate motor health status and noise types. These conditions were designed to evaluate the impact of motor health status and noise conditions on classification performance. In all conditions, classification was performed using MobileNet V2 [17], Inception V3 [18], and a custom CNN model.

The architecture of the custom CNN model consists of three convolutional layers with increasing filter sizes (32, 64, and 128 filters, respectively) and a kernel size of 3×3. Each convolutional layer employs the ReLU activation function and is followed by a max-pooling layer with a pool size of 2×2 to reduce spatial dimensions and computational complexity. The feature maps generated by the convolutional layers are flattened and passed to a dense layer comprising 128 neurons with ReLU activation to learn high-level features. To prevent overfitting, a dropout layer with a rate of 0.5 is applied. Finally, the output layer uses the softmax activation function to produce probabilities for each of the three classes, enabling multi-class classification.

- **Condition-1:** A 3-class classification focused solely on assessing motor health status.
- **Condition-2:** A 15-class classification aimed at evaluating both motor health status and noise types simultaneously.
- **Condition-3:** A 12-class classification where data from the "stresstest" noise type was excluded. This adjustment was made because the number of samples under the "stresstest" condition was significantly lower compared to other noise conditions, ensuring a more balanced dataset for classification.

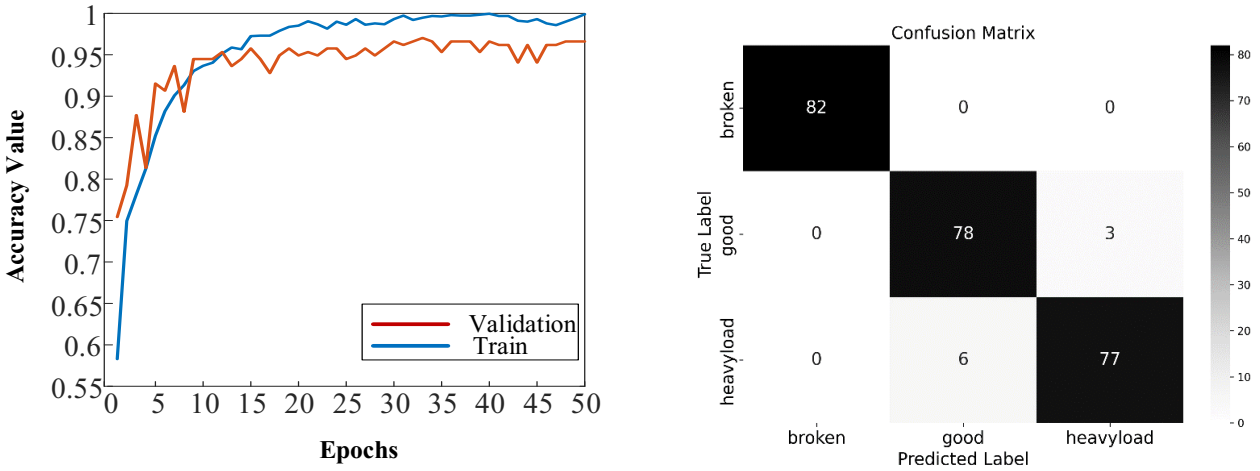

a) b)

Fig. 2: Accuracy graph (a) and Confusion matrix for Condition-1 (b).

Figure 2 illustrates the performance of the custom CNN model for 3-class classification. Figure 2(a) presents the variation of accuracy values during training and validation phases, indicating that the model achieved an accuracy level above 95%. Figure 2(b) displays the confusion matrix, which shows the percentage of correctly classified samples for each class. For instance, all samples in the "broken" class were correctly classified, while 3 samples in the "good" class and 6 samples in the "heavyload" class were misclassified. These results demonstrate the model's strong performance in accurately distinguishing between classes.

Table 2 shows the class-based performance metrics of the CNN model for the 3-class classification task. The metrics cover precision, recall, F1-score, and accuracy for each class and overall performance. The "broken" class achieved 100% in all metrics, indicating that all samples in this class were classified correctly. The "good" and "heavyload" classes achieved precision, recall, and F1-scores above 92%, with accuracy values of 96.34% for both classes. The overall performance metrics suggest that the model performs consistently across all classes, with an overall precision of 96.37%, recall of 96.36%, F1-score of 96.34%, and accuracy of 96.34%.

Table 2: Class-based performance metrics for Condition-1.

Class	Precision	Recall	F1-Score	Accuracy
Broken	100.00	100.00	100.00	100.00
Good	92.86	96.30	94.55	96.34
Heavyload	96.25	92.77	94.48	96.34
Overall	96.37	96.36	96.34	96.34

Figure 3 illustrates the t-SNE visualization of the data distribution across the three classes. The visualization reduces the high-dimensional feature space into two dimensions, enabling a clear representation of the class separability. The clusters formed in the plot indicate that the samples belonging to the same class are grouped closely together, while different classes are distinctly separated. This suggests that the features extracted by the model effectively differentiate between the classes, supporting the classification performance observed in other metrics.

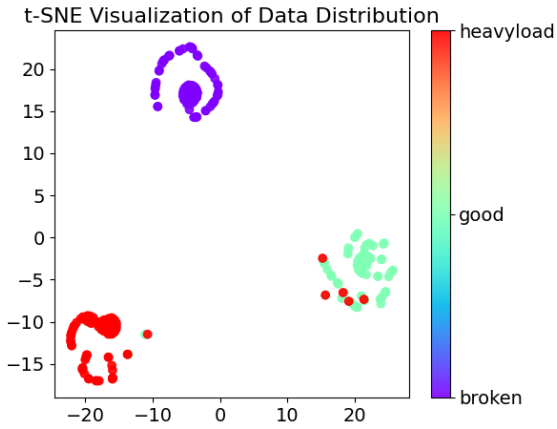

Fig. 3: t-SNE visualization.

Figure 4 illustrates misclassified samples belonging to the “good” class. Each plot represents a sample from the “good” class that was incorrectly predicted as “heavyload”. The probability scores for each class are provided above the respective plots, showing the model's confidence in its predictions. Despite belonging to the “good” class, the model assigns a higher probability to the “heavyload” class, leading to misclassification. All misclassified samples were generated under the “stresstest” noise type, which may have introduced patterns that resemble features of the “heavyload” class, increasing the likelihood of confusion. This observation suggests that the “stresstest” noise type could have a significant impact on the model’s feature extraction and classification process, highlighting the importance of further analysis to mitigate the effects of such noise on classification accuracy.

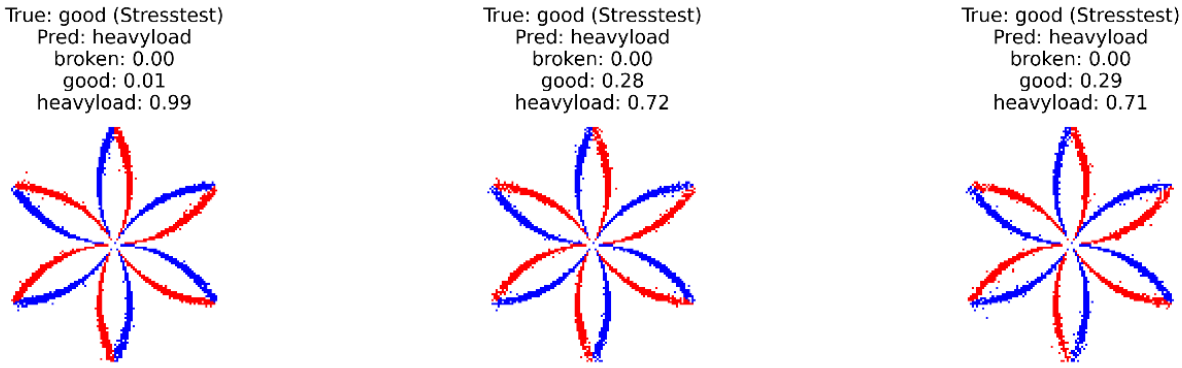

Fig. 4: Misclassified samples belonging to the good class.

Figure 5 shows misclassified samples belonging to the “heavyload” class under different noise types. Each visualization represents a sample incorrectly predicted as belonging to the “good” class. Notably, most misclassifications occurred under the “stresstest” noise type. In some cases, the model predicted the “good” class with high confidence, while in one instance, an equal probability distribution between the “good” and “heavyload” classes (0.50 each) was observed. This suggests that the “stresstest” noise conditions may have introduced uncertainty in the model's predictions. Under the “atmo” and “talking” noise types, the model predicted the “good” class with high confidence, leading to misclassifications.

These observations indicate that the “stresstest” noise type poses a greater challenge for the model, highlighting the need for targeted solutions such as improved noise handling techniques or additional feature engineering strategies to enhance classification accuracy.

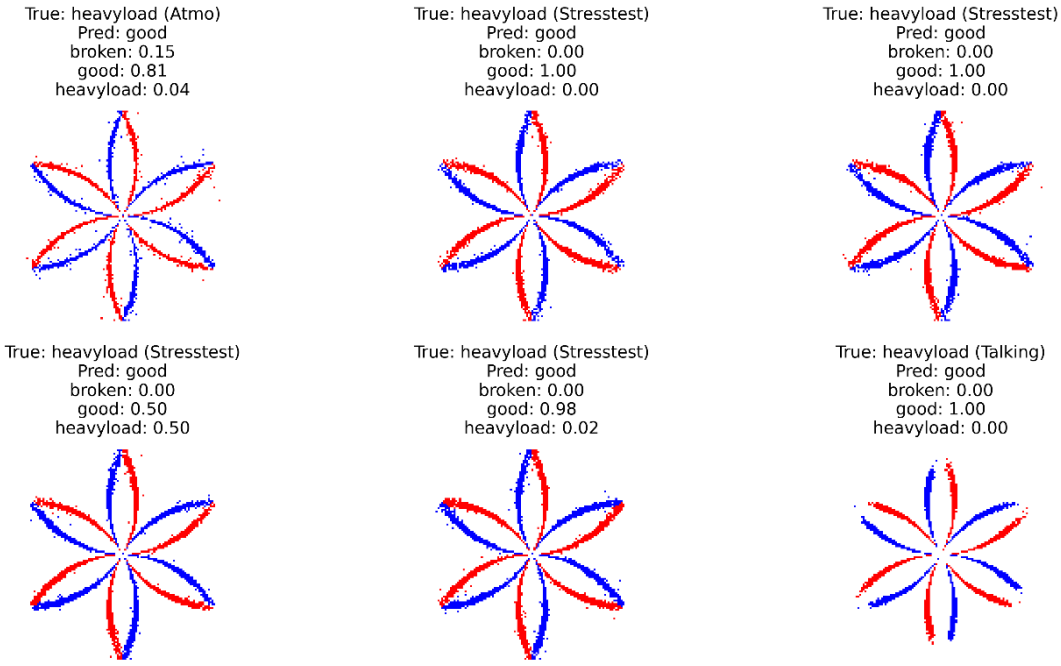

Fig. 5: Misclassified samples belonging to the heavyload class.

Performance metrics of the models on different conditions is given in Table 3. In Condition-1, all models achieved their highest performance, with Custom CNN obtaining the best metrics. In Condition-2, performance decreased significantly due to the increased complexity, where MobileNet achieved the highest accuracy and F1-score. Condition-3 led to improved performance compared to Condition-2, as MobileNet again outperformed with 81.39% accuracy and 80.41% F1-score. These results highlight that the complexity of the classification task and data imbalance significantly impact model performance. While Custom CNN excelled in simpler tasks (Condition-1), MobileNet demonstrated robustness across varying conditions, whereas InceptionV3 consistently lagged.

Table 3: Performance metrics of the models on different conditions.

Conditions	Models	Precision	Recall	F1-Score	Accuracy
Condition-1	MobileNet	95.93	95.91	95.91	95.93
	InceptionV3	94.56	97.15	94.28	94.31
	Custom CNN	96.37	96.36	96.34	96.34
Condition-2	MobileNet	73.28	72.56	71.66	76.02
	InceptionV3	70.87	66.64	65.60	73.17
	Custom CNN	73.09	68.75	68.60	73.58
Condition-3	MobileNet	84.94	80.40	80.41	81.39
	InceptionV3	75.12	70.84	68.60	73.59
	Custom CNN	81.63	75.85	75.94	77.49

Figure 6a shows the confusion matrix for MobileNet under Condition-2, which involves a 15-class classification combining motor health status and noise types. The matrix provides detailed insights into the model's predictions for each class. It can be observed that when the motor health condition is “good”, the noise types are classified more accurately. However, for the “broken” and “heavyload” health conditions, distinguishing between different noise types is more challenging. This highlights the need for further refinement in feature extraction or implementing noise mitigation strategies to improve the classification of noise types, particularly under “broken” and “heavyload” health conditions.

Figure 6b presents the confusion matrix for MobileNet under Condition-3, where the “stresstest” noise type has been excluded, resulting in a 12-class classification. The exclusion of the “stresstest” noise type appears to have improved the model's performance overall. However, the overlap in certain noise types under “broken” and “heavyload” conditions suggests that further refinement in feature extraction may be necessary to enhance classification accuracy for these health conditions.

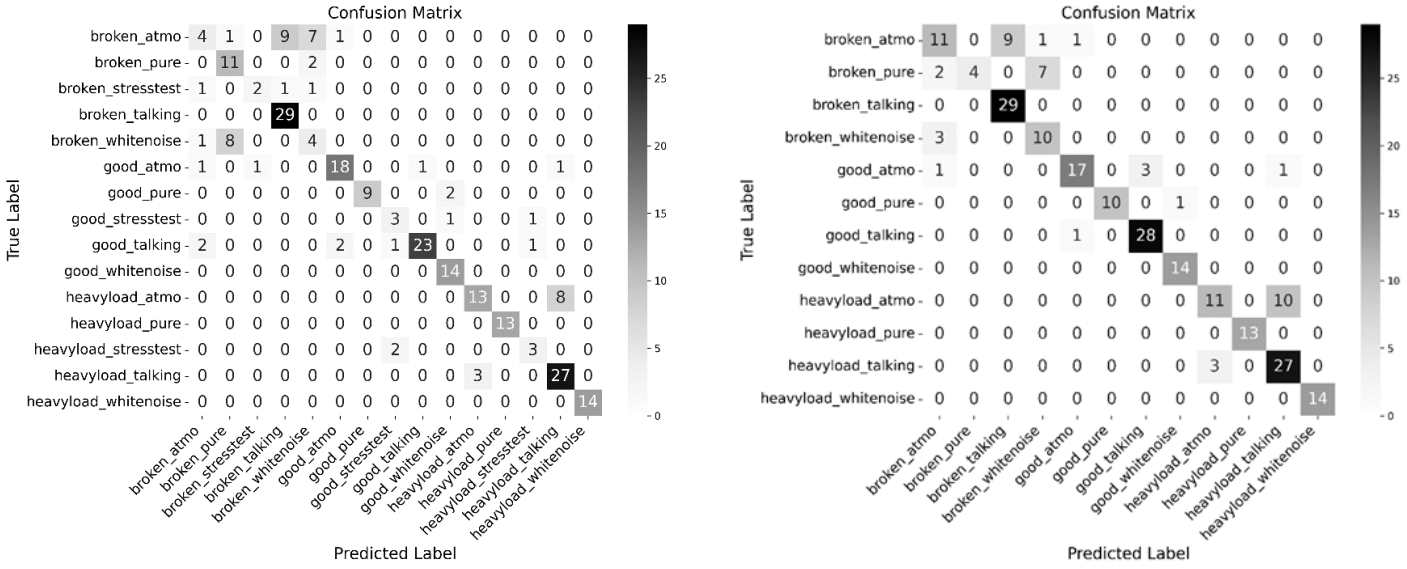

a) b)

Fig. 6: Confusion matrices of MobileNet for Condition-2 (a) and Condition-3 (b).

4. Conclusion

In this study, acoustic data obtained from a brushless DC motor under different health and noise conditions were converted into SDP images. Using these images, the classification of the motor’s health status was performed with CNN-based models. The CNN models were trained under various noise conditions to better adapt to real-world scenarios. In health status classification, accuracy rates of 94.31%, 95.93%, and 96.34% were achieved with InceptionV3, MobileNet, and Custom CNN models, respectively. These results demonstrate the feasibility of using SDP images with CNN-based models for fault classification in motors. However, when the noise type is also included in the classification along with the health status, accuracy rates drop to as low as 73.17%. While Custom CNN provided the best results for health status classification alone, MobileNet emerged as the most successful model in more challenging scenarios where noise types were also included in the classification. In future studies, different feature extraction techniques will be applied to the acoustic data, and various representations of the data will be combined in multimodal structures to improve classification accuracy.

Acknowledgements

This research was funded by the Research and Development Sector at the Technical University of Sofia, Bulgaria under Project No. 242PD0002-08/2024.

References

[1] A. Hughes and B. Drury, 'Electric motors and drives: fundamentals, types and applications", 2019.
[2] R. Crowder, "Electric drives and electromechanical systems: applications and control", Butterworth-Heinemann, 2019.
[3] M.-A Sheikh, S.-T. Bakhsh, M. Irfan, N.-B. Nor and G. Nowakowski, "A review to diagnose faults related to three-phase industrial induction motors", Journal of Failure Analysis and prevention, 2022.
[4] J. Ma, Y. Xue, Q. Han, X. Li, C. Yu, "Motor Bearing Damage Induced by Bearing Current: A Review", Machines, 2022.
[5] T. Garcia-Calva, D. Morinigo-Sotelo, V. Fernandez-Cavero and R. Romero-Troncoso, "Early detection of faults in induction motors—A review", Energies. 2022.
[6] J. Zarei, M. Tajeddini and H. Karimi, "Vibration analysis for bearing fault detection and classification using an intelligent filter", Mechatronics, Volume 24, Issue 2, 2014, ISSN 0957-4158, DOI: https://doi.org/10.1016/j.mechatronics.2014.01.003.
[7] I. Areias, L. Borg da Silva, E. Bonaldi, L. E. de Lacerda de Oliveira, G. Lambert-Torres, V. Bernardes, "Evaluation of Current Signature in Bearing Defects by Envelope Analysis of the Vibration in Induction Motors", Energies 2019, 12, 4029, DOI: https://doi.org/10.3390/en12214029.
[8] M. Yurdakul and S. Tasdemir. "Acoustic Signal Analysis with Deep Neural Network for Detecting Fault Diagnosis in Industrial Machines." arXiv preprint arXiv:2312.01062 (2023).
[9] N. Sergin, J. Huang, T. Chang and H. Yan, "Image-based novel fault detection with deep learning classifiers using hierarchical labels." IISE Transactions, 56(10), 1112–1130, https://doi.org/10.1080/24725854.2024.2326068.
[10] M.-H. Wang; Z.-H. Lin and S.-D. Lu, "A Fault Detection Method Based on CNN and Symmetrized Dot Pattern for PV Modules", Energies, 2022, DOI: https://doi.org/10.3390/en15176449.
[11] M.-H. Wang, J.-X. Hong and S.-D. Lu, "Fault Diagnosis of Lithium Battery Modules via Symmetrized Dot Pattern and Convolutional Neural Networks", Sensors, 2024, DOI: 10.3390/s25010094. 7
[12] H. Wang, J. Xu and R. Yan, "Bearing Fault Diagnosis Based on Visual Symmetrized Dot Pattern and CNNs," 2019 IEEE International Instrumentation and Measurement Technology Conference (I2MTC), Auckland, New Zealand, 2019, pp. 1-6, doi: 10.1109/I2MTC.2019.8827101.
[13] W. Cui, G. Meng, T. Gou, A. Wang, R. Xiao and X. Zhang, "Intelligent Rolling Bearing Fault Diagnosis Method Using Symmetrized Dot Pattern Images and CBAM-DRN", Sensors, 2022, DOI: 10.3390/s22249954.
[14] L. Huang, J. Wen, Y. Yang, L. Chen and G. Shen, "A Visual Fault Detection Method for Induction Motors Based on a Zero-Sequence Current and an Improved Symmetrized Dot Pattern", Entropy 2022, DOI: https://doi.org/10.3390/e24050614.
[15] N. Yordanov, M. Zhilevski and M. Mikhov, "Fault Detection in Electric Motors using Acoustic Signals and Image Classification", 2024 International Conference on Applied and Theoretical Electricity (ICATE), IEEE Xplore, 2024, Craiova, Romania, pp. 1-6, DOI: 10.1109/ICATE62934.2024.10749208
[16] S. Grollmisch, J. Abeßer, J. Liebetrauand and H. Lukashevich, "IDMT-ISA-electric-engine dataset", Zenodo, Sep. 01, 2019. DOI: 10.5281/zenodo.7551261.
[17] M. Sandler, A. Howard, M. Zhu, A. Zhmoginov, L.C. Chen, "Mobilenetv2: Inverted residuals and linear bottlenecks", In Proceedings of the IEEE conference on computer vision and pattern recognition, 2018, (pp. 4510-4520). https://doi.org/10.48550/arXiv.1801.04381.
[18] C. Szegedy, V. Vanhoucke, S. Ioffe, J. Shlens, Z. Wojna, "Rethinking the inception architecture for computer vision", In Proceedings of the IEEE conference on computer vision and pattern recognition, 2016, (pp. 2818-2826).